J. Fluid Mech. (2005), *vol.* 541, *pp.* 345–370.
doi:10.1017/S0022112005006063 Printed in the United Kingdom

Short surface waves on surface shear

By X. ZHANG

Scripps Institution of Oceanography, University of California, San Diego La Jolla, CA 92093-0213, USA

(Received 7 July 2004 and in revised form 16 March 2005)

The problem of short wind waves propagating on surface wind drift is considered here. Under the assumption of small monochromatic surface waves on a steady and horizontally uniform surface shear of an inviscid fluid, the governing equation becomes the well-known Rayleigh instability equation. Perturbation solutions exist for the surface-wave problem; however, the conditions for these approximations are violated in the case of short wind waves on wind drift shear. As an alternative approach, the piecewise-linear approximation (PLA) is explored. A proof is given for the rate of convergence of the piecewise-linear approximation for solving the Rayleigh equation without limitations on boundary conditions. The artificial modes of the piecewise-linear flow system are also discussed. The method is numerically efficient and highly accurate. Applying this method, the linear instability of various boundary-layer flows is examined. Short waves propagating with surface shear-flows are stable, while it is possible for waves that are travelling against a shear current to become unstable when the surface speed of the shear is greater than the wavespeed in stagnant fluid. PLA is also applied to examine the applicability of other perturbation approaches to the problem of propagation of short waves on wind drift shear. It is found that the existing approximations cannot fit the whole range of short wind waves. To bridge the gap, new approximations are derived from an implicit form of the exact dispersion relation based upon the variational principle.

1. Introduction

The mean wind drift and the vertical structure of currents near the sea surface have long been subjects of intense study among oceanographers. Unlike well-established theories and observations on solid wall boundary layers, the understanding of wave boundary layers is still considered to be inadequate, owing to both the complexity of the problem and the difficulty in making reliable observations. Naturally, attempts have been made to extend the similarity theories of solid wall boundary layers to wave boundary layers. The wall boundary-layer analogy can be tested if the predicted surface shear profile and turbulent dissipation match with field observations. However, the precise form of the actual current near the surface remains uncertain (Terray *et al.* 1996). Hampered by the motions of surface waves, direct measurement of flows within the top metre of the ocean surface has thus far been a serious challenge. Since the surface currents affect the surface waves, a possible alternative is to use surface waves as natural tracers to measure surface currents indirectly, such as by RH radar sounding and optical imaging of ocean surface currents. To resolve surface shear at a fine scale, different surface-wave components, long waves and short waves, have to be measured. There are complications when surface shears are indirectly calculated from the measurements of propagation velocities of short waves. Here, we will focus on the

forward calculation problem of calculating the propagation speed of short waves on a steady current with a realistic vertical profile when the wavelength is comparable to the depth of the surface shear layer; a situation in which the existing perturbation methods may fail.

Under the assumptions of small monochromatic surface waves on a steady and horizontally uniform surface shear flow $\mathscr{U}(z)$ of an inviscid fluid, it has been shown that the well-known Rayleigh equation, which was derived from the classical study of the instability of shear flows, becomes the governing equation of the motion. Here, we use the governing equation for vertical wave motion, with the notations used by Shrira (1993):

$$(c-\mathscr{U})(\mathscr{W}''-k^2\mathscr{W})+\mathscr{U}''\mathscr{W}=0. \tag{1.1}$$

It is assumed that the vertical velocity of a small-amplitude wave has the form of $\mathscr{W}(z)\exp(\mathrm{i}(\boldsymbol{k}\cdot\boldsymbol{x}-ct))$ where $\boldsymbol{k}$ is the wavenumber and is real, and c is the wave propagation speed in the fixed frame of reference. The primed quantities are the derivatives with respect to the vertical axis z, and the axis is pointed upward. The current velocity component, $\mathscr{U}$, is the projection of $\mathscr{U}$ in the wavenumber direction and is given. The equation for waves is equivalent to the linearized vorticity equation for a small periodic disturbance (Thompson 1949). The combined kinematic and dynamical boundary condition at the mean free surface is

$$(c-\mathscr{U})^2\mathscr{W}'+\left[\mathscr{U}'(c-\mathscr{U})-kc_o^2\right]\mathscr{W}=0|_{z=0}, \tag{1.2}$$

where $c_o=(g/k+Tk)^{1/2}$ is the linear phase speed of surface waves in deep water in the absence of a current. The motion vanishes at the bottom boundary:

$$\mathscr{W}=0|_{z=-H}. \tag{1.3}$$

The exact analytical solutions to the problem are known for a very limited number of specific current profiles: linear (Thompson 1949), exponential (Abdullah 1949), and for $z^{1/7}$ (Lighthill 1953; Fenton 1973). For realistic arbitrary current profiles, approximate solutions are used. The HF radio can sense ocean surface waves in a range of a few metres to 100 m in wavelength, corresponding to propagation speeds larger than $1\,\mathrm{m\,s^{-1}}$. Surface currents and their vertical derivatives are normally much smaller than the speed of these long waves. In these cases, $(c-\mathscr{U})\approx c$ and the last term in (1.1) is also relatively small, and the solution from the equation that the first term equals zero plus a perturbation adjustment is a valid approximation (Stewart & Joy 1974; Skop 1987; Kirby & Chen 1989). Assuming that the characteristic depth and speed of the surface shear flow are D and U_o, the Froude number of the shear flow can be defined as:

$$Fr=\frac{U_o}{\sqrt{gD}}.$$

The relative scales of the wave and the current can be characterized by the non-dimensional factors:

$$\gamma=\frac{U_o}{c_o},\quad s=kD.$$

There are three different length scales involved: for the wave $(1/k)$, shear (D), and water depth (H), and two velocity scales for wave (c_o) and shear flow (U_o). Normally, the water depth is either the same as the shear-layer depth or infinity. Scaling wave and current separately, Shrira (1993) derived the following non-dimensional forms of

(1.1)–(1.3):

$$(c-\gamma\mathscr{U})(\mathscr{W}''-\mathscr{W})+\frac{\gamma}{s^2}\mathscr{U}''\mathscr{W}=0, \tag{1.4}$$

$$s(c-\gamma\mathscr{U})^2\mathscr{W}'+[\gamma\mathscr{U}'(c-\gamma\mathscr{U})-s]\mathscr{W}=0|_{z=\eta}, \tag{1.5}$$

$$\mathscr{W}=0|_{z=-kH}. \tag{1.6}$$

When $\varepsilon=\gamma/s^2$ is less than 1, an analytical solution is found as a series in $\varepsilon^m\mathscr{W}_{(m)}$ for arbitrary current profiles. The corresponding dispersion relation is found as a function of $R(c)$ (Shrira 1993):

$$(c-\gamma\mathscr{U}_o)^2k(1-\varepsilon R)+\left[\mu\mathscr{U}'_o(c-\gamma\mathscr{U}_o)-kC_o^2\right](1+\varepsilon R)=0, \tag{1.7}$$

where

$$R=-\frac{1}{2k}\int_{-\infty}^{0}f(z)\exp(kz)\,\mathrm{d}z+\frac{\varepsilon}{4k^2}\int_{-\infty}^{0}f(z)\exp(kz)\,\mathrm{d}z\int_{-\infty}^{0}f(z_1)\exp(k|z-z_1|)\,\mathrm{d}z_1+\cdots,$$

the summation over a series of functions of c in power of ε, and can be calculated numerically for any given surface current profile. Here $f(z)=\mathscr{U}(z)''/(c-\gamma\mathscr{U}(z))$.

When γ is small, i.e. for long waves, (1.4) can further be reduced to a convenient form (Stewart & Joy 1974), which yields the dispersion relation:

$$c=c_o-2k\int_{\infty}^{0}\mathscr{U}\,\mathrm{e}^{2kz}\,\mathrm{d}z+O(\varepsilon). \tag{1.8}$$

Equation (1.8) and higher-order approximations have been tested against the known analytic surface current profiles (Skop 1987; Kirby & Chen 1989), and found to be a very close approximation for long surface waves. In terms of finding an analytic solution of (1.4), the requirement of $\varepsilon<1$ remains a limitation for arbitrary current profiles.

The other approach, without the limitation of $\varepsilon<1$, is based on the piecewise-linear approximation (PLA) of velocity profiles, as was suggested by Thompson (1949). A realistic smooth flow profile is approximated by many piecewise-linear ones, thus representing the flow as a set of constant vorticity layers. This approximation reduces the problem to an algebraic equation that can easily be treated numerically (Gertsenshtein, Romashova & Chernyavski 1988). However, the convergence of the solution using the piecewise-linear approximation to the solution of the corresponding continuous problem has not yet been rigorously proved (Gertsenshtein 1970). Thus, it is important to understand the degree to which the approach works and when it breaks down. Most of its applications are still limited to two or three layers, both for simplicity and for the ability to qualitatively explain some shear-flow instability problems (Gossard & Hooke 1975; Pedlosky 1982; Longuet-Higgins 1998). It has been recognized that two or three linear layers cannot quantitatively represent the problem (Caponi *et al.* 1991; Engevik 2000). Even if we assume that the PLA solution will converge toward the real solution as the number of layers increases, it is known that the number of eigenmodes can also increase rapidly (Shrira & Sazonov 2001), a circumstance that is difficult to interpret. Thus, the results from PLA with many flow layers have so far been set aside by many. These fundamental problems of PLA must be solved before it will be of much use.

In this paper, we will first prove the rate of convergence of the piecewise-linear approximation. Then, we will discuss the dispersion relation in some detail for mode selection and address the problem of artificial eigenmodes. The first application is to find the neutral modes of different surface shear flows as a function of wavenumber.

These neutral modes determine the boundaries of the linear instability regions. The second task is to evaluate the applicability of the existing and newly proposed perturbation approximations to the problem of short surface waves propagating on the surface at the upper boundary of the shear current. The piecewise-linear approximation is highly accurate as the number of the flow layers increases, at the expense of increasing difficulty in inverse calculation. On the other hand, the perturbation expansions have clear advantages for formulating an inverse calculation, providing that their applicability can now be checked by PLA.

2. Piecewise-linear approximation method

A vertically continuous surface shear flow, $\mathscr{U}(z)$, is first approximated by n layers of linear velocity, $U(z)$, which requires continuity of velocity at the interfaces:

$$U(z) = U_i - b_i(z_i - z) = \mathscr{U}(z_i) - \frac{\mathscr{U}(z_i) - \mathscr{U}(z_{i+1})}{z_i - z_{i+1}}(z_i - z), \quad \text{for} \quad z_{i+1} < z < z_i, \quad i = 0, \ldots, n-1, \tag{2.1a}$$

$$U_o = \mathscr{U}(z_o), \quad z_o = 0, \tag{2.1b}$$

$$U_n = \mathscr{U}(-D), \tag{2.1c}$$

$$z_n = -D. \tag{2.1d}$$

Here the z-axis points upward with its origin at the mean water level. All quantities from this point on, unless specified, are non-dimensionalized by wave scales, where the velocity scale is c_o, and the length scale is k^{-1}. This implies that although the waves considered here are modified or distorted by the surface shear, their basic characteristic remains. Since the piecewise-linear approximation is not limited by the condition $\varepsilon < 1$, we will not introduce the current scale until later, when comparing different approaches. This simplifies the formulation of the convergence proof. Equation (2.1) in non-dimensional form is therefore:

$$U(z) = U_i - b_i(z_i - z) = \mathscr{U}(kz_i) - \frac{\mathscr{U}(kz_i) - \mathscr{U}(kz_{i+1})}{k(z_i - z_{i+1})}(kz_i - kz), \quad \text{for} \quad z_{i+1} < z < z_i, \quad i = 0, \ldots, n-1, \tag{2.2a}$$

$$U_o = \mathscr{U}(z_o), \;\; z_o = 0, \tag{2.2b}$$

$$U_n = \mathscr{U}(-s), \tag{2.2c}$$

$$z_n = -kD = -s. \tag{2.2d}$$

We can find the wave solution $W(z)$ for the piecewise-linear velocity profile and examine how close it is to the wave solution $\mathscr{W}(z)$ of the corresponding continuous profile, if it exists. We will prove that $W(z)$ converges to $\mathscr{W}(z)$ as the number of layers becomes infinite, and also give an estimate of the deviation of $W(z)$ from $\mathscr{W}(z)$ in terms of the layer thickness.

At the mean free surface $z_o = 0$, the boundary condition can be derived by combining the kinematic and dynamic boundary conditions:

$$(c - \gamma U_o)^2 W' + [\gamma U_o'(c - \gamma U_o) - 1]W = 0|_{z=z_o}, \tag{2.3}$$

where $\gamma = U_o/c_o$. Our non-dimensional Rayleigh equation is:

$$(c - \gamma U)(W'' - W) + \gamma U'' W = 0. \tag{2.4}$$

The shear current below depth $z_n = -s$ is weak and the solution can be found with the perturbation method mentioned earlier. At the first order, for example, it is in the form of $\sinh(k(H+z))$ for finite depth flows or e^{kz} for infinite depth flows. Here we assume that $\mathscr{W}(z<-s)$ is known with an unknown constant of proportionality. The lower boundary condition is therefore:

$$W|_{z=-kD} = A_n \sinh(k(H-D)). \tag{2.5}$$

Since the second derivative is zero everywhere except at layer interfaces for $U(z)$, the governing equation reduces to a simple form for almost every point within each of the layers:

$$W'' - W = 0 \quad \text{when } z_i < z < z_{i+1}, \quad i = 0, \ldots, n-1. \tag{2.6}$$

At points where $\gamma U(z_c) = c$, $W'' - W$ does not have to vanish:

$$W'' - W = a\delta(c - \gamma U). \tag{2.7}$$

Here, $\delta(\bullet)$ is a delta function. However, the solution of (2.6) would normally include the solution of (2.7). A departure from the continuous velocity profile happens when $\mathscr{U}'' \neq 0$ at $\gamma U(z_c) = c$. We postpone discussion of this case until later sections. At the layer interfaces, we require continuity of the vertical velocity and of the horizontal pressure gradient, or the vorticity jump condition:

$$W(z_i + \Delta z) - W(z_i - \Delta z) \to 0, \quad \text{as } \Delta z \to 0, \tag{2.8a}$$

$$(c - \gamma U_i)[W'(z_i + \Delta z) - W'(z_i - \Delta z)] = -\gamma(U'(z_i + \Delta z) - U'(z_i - \Delta z))W(z_i) \quad \text{as } \Delta z \to 0. \tag{2.8b}$$

Also, we must consider the case of $c = \gamma U_i$. When $U'(z_i + \Delta z) - U'(z_i - \Delta z) \neq 0$, it is required by (2.8) that the solutions of non-singular equations be zero at the interface $W(z_i) = 0$. This is a departure from the continuous current profile when $\mathscr{U}'' = 0$ at the interface. When $\mathscr{U}'' \neq 0$, $U'(z_i + \Delta z) - U'(z_i - \Delta z)$ is normally not zero, and the two systems are consistent.

In general, the system of (2.8) violates the original governing equation at the layer interfaces, which can be written in a limiting form as:

$$(c - \gamma U_i)\left\{\frac{\left[W'\left(z_i + \tfrac{1}{2}\Delta \boldsymbol{z}\right) - W'\left(z_i - \tfrac{1}{2}\Delta z\right)\right]}{\Delta z} - W(z_i)\right\} = -\gamma \frac{\left(U'\left(z_i + \tfrac{1}{2}\Delta z\right) - U'\left(z_i - \tfrac{1}{2}\Delta z\right)\right)}{\Delta z} W(z_i) \quad \text{as } \Delta z \to 0. \tag{2.9}$$

Comparing (2.9) to (2.8), the extra term $W(z_i)$ here shows that a correction to the interface boundary condition of (2.8) is required. The correction is necessary for the later proof of convergence. The source of this correction is from expanding $W(z)$ further in the power of Δz:

$$W(z) = W_{(0)}(z) + (\Delta z)^1 W_{(1)}(z) + (\Delta z)^2 W_{(2)}(z) + \cdots. \tag{2.10}$$

The dynamically consistent system equation for the expanded $W(z)$ is:

$$W''_{(m)} - W_{(m)} = 0 \quad \text{when } z_i < z < z_{i+1}, \quad i = 0, \ldots, n-1, m = 0, 1, \ldots. \tag{2.11}$$

$$W_{(m)}\left(z_i + \tfrac{1}{2}\Delta z\right) - W_{(m)}\left(z_i - \tfrac{1}{2}\Delta z\right) = 0 \quad \text{as } \Delta z \to 0, \tag{2.12a}$$

$$\left.\begin{aligned}
&(c-\gamma U_i)\left[W'_{(0)}\left(z_i+\tfrac{1}{2}\Delta z\right)-W'_{(0)}\left(z_i-\tfrac{1}{2}\Delta z\right)\right]\\
&\quad=-\gamma\left[U'\left(z_i+\tfrac{1}{2}\Delta z\right)-U'\left(z_i-\tfrac{1}{2}\Delta z\right)\right]W_{(0)}(z_i)\quad\text{as }\Delta z\to 0,\\
&(c-\gamma U_i)\left[W'_{(m)}\left(z_i+\tfrac{1}{2}\Delta z\right)-W'_{(m)}\left(z_i-\tfrac{1}{2}\Delta z\right)-W_{(m-1)}\right]\\
&\quad=-\gamma\left[U'\left(z_i+\tfrac{1}{2}\Delta z\right)-U'\left(z_i-\tfrac{1}{2}\Delta z\right)\right]W_{(m)}(z_i),\quad m>0\quad\text{as }\Delta z\to 0.
\end{aligned}\right\}\tag{2.12b}$$

$$(c-\gamma U_o)^2\,W'_{(m)}\big|_{z=z_o}+[\gamma U'_o(c-\gamma U_o)-1]W_{(m)}|_{z=z_o}=0|_{z=z_o}.\tag{2.13}$$

To prove that as the number of layers tends toward infinity, the solution of $W(z)=\sum_{m=0}(\Delta z)^m W_{(m)}(z)$ converges to the solution $\mathscr{W}(z)$, for the corresponding continuous current profile $\mathscr{U}$, we let $\Delta z=s/n$ (or in the dimensional form $\Delta z=D/n$) be equal to the layer thickness. Taking all layers to have the same thickness simplifies the formulation, but is not necessary. Multiplying the vorticity jump condition to all orders by (Δz) to the power of the order, summing them all up, and dividing by Δz, we obtain:

$$\begin{aligned}
&(c-\gamma U_i)\left\{\sum_{m=0}(\Delta z)^m\frac{\left[W'_{(m)}\left(z_i+\tfrac{1}{2}\Delta z\right)-W'_{(m)}\left(z_i-\tfrac{1}{2}\Delta z\right)\right]}{\Delta z}-\frac{\Delta z}{\Delta z}\sum_{m=0}(\Delta z)^m W_{(m)}\right\}\\
&\quad=-\gamma\frac{\left[U'\left(z_i+\tfrac{1}{2}\Delta z\right)-U'\left(z_i-\tfrac{1}{2}\Delta z\right)\right]}{\Delta z}\sum_{m=0}(\Delta z)^m W_{(m)}(z_i),\quad \Delta z\to 0.
\end{aligned}\tag{2.14}$$

Note that

$$\begin{aligned}
\left[U'\left(z_i+\tfrac{1}{2}\Delta z\right)-U'\left(z_i-\tfrac{1}{2}\Delta z\right)\right]&=\left[\frac{\mathscr{U}(z_{i-1})-\mathscr{U}(z_i)}{z_{i-1}-z_i}-\frac{\mathscr{U}(z_i)-\mathscr{U}(z_{i+1})}{z_i-z_{i+1}}\right]\\
&=\left[\mathscr{U}'\left(z_i+\tfrac{1}{2}\Delta z\right)-\mathscr{U}'\left(z_i-\tfrac{1}{2}\Delta z\right)\right]+O(\Delta z^2).
\end{aligned}$$

If the second derivative, $W''_{(m)}(z)$ exists at the layer interfaces, then the limit of (2.14) is

$$(c-\gamma\mathscr{U})\left(W''_{(0)}+W_{(0)}\right)+\gamma\mathscr{U}''W_{(0)}=0,\quad z=z_i.\tag{2.15}$$

The higher-order terms $W_{(m)}(z)$ become insignificant as $\Delta z\to 0$. The solution $W_{(0)}(z)$ from a piecewise-linear system may not necessarily be second-order differentiable at the layer interfaces. In this case, we can introduce a second-order differentiable function $\hat{\mathscr{W}}_n(z_i)$ whose values at the interfaces are specified by:

$$\begin{aligned}
&\hat{\mathscr{W}}_n(z_i)=W_{(0)}(z_i),\\
&\hat{\mathscr{W}}''_n(z_i)=-\left(\frac{\gamma\mathscr{U}''(z_i)}{(c-\gamma\mathscr{U}(z_i))}-1\right)W_{(0)}(z_i),
\end{aligned}\tag{2.16}$$

$i=1,\ldots,n-1$, in addition to the bottom and surface boundary conditions:

$$\hat{\mathscr{W}}_n(z_0)=W_{(0)}(z_0),\quad \hat{\mathscr{W}}'_n(z_0)=W'_{(0)}(z_0),\quad \hat{\mathscr{W}}_n(z_n)=W_{(o)}(z_n),\tag{2.17}$$

so that at the layer interfaces $z=z_i, i=1,\ldots,n-1$:

$$(c-\gamma\mathscr{U})(\hat{\mathscr{W}}''+\hat{\mathscr{W}})+\gamma\mathscr{U}''\hat{\mathscr{W}}=0.\tag{2.18}$$

In the limit of $\Delta z\to 0$, the functional series $\{\hat{\mathscr{W}}_{(n)}(z)\}$ converges to $\mathscr{W}(z)$ as long as the boundary conditions are satisfied. Since $W_{(0)}(z_i)=\hat{\mathscr{W}}_n(z_i)$, $i=0,\ldots,n$, this further leads to

$$W_{(0)}(z)\to\mathscr{W}(z),\quad \Delta z\to 0.\tag{2.19}$$

An example of such $\{\hat{\mathscr{W}}_{(n)}(z)\}$ can be a polynomial of order $2n$. The $2n+1$ coefficients are specified by the $2n+1$ equations of (2.16) and (2.17). In practice, the particular forms of $\{\hat{\mathscr{W}}_{(n)}(z)\}$ and $W_{(m)}(z)$, for $m>0$, are not particularly important.

All that remains at this stage is to construct a solution $W_{(0)}(z)$. Following the suggestion by Thompson (1949), let the piecewise-linear solution be in the form:

$$W(z) = A_i \sinh(z - z_{i+1}) + W(z_{i+1})\cosh(z - z_{i+1}),\ z_i > z > z_{i+1},$$
$$A_i = \frac{W(z_i) - W(z_{i+1})\cosh(z_i - z_{i+1})}{\sinh(z_i - z_{i+1})}. \tag{2.20}$$

This satisfies (2.11) and is continuous at the layer interfaces. The n constants, $W(z_i), i = 0, \ldots, n-1$, and wave speed c ($n+1$ unknown) are to be determined by the vorticity jump condition at $n-1$ layer interfaces (2.12), the free-surface boundary condition of (2.3), and the bottom boundary condition (2.5).

In the same fashion, we can estimate how accurate the piecewise-linear approximation is for a given number of layers. Let $\mathscr{C}$, a subspace of complex numbers, denote the set of all the eigenvalues of the Rayleigh equation system with a continuous shear profile. The corresponding eigenfunction is $\mathscr{W}(z,c)$, which belongs to a certain space of function $\mathscr{F}$. The surface current, any $c \in \mathscr{C}$, and the corresponding $\mathscr{W}(z,c)$ are expanded as:

$$\mathscr{U}''(z) = \frac{1}{\Delta z}\left[\frac{\mathscr{U}(z+\Delta z) - \mathscr{U}(z)}{\Delta z} - \frac{\mathscr{U}(z) - \mathscr{U}(z-\Delta z)}{\Delta z}\right] + \tfrac{1}{12}\mathscr{U}''''(z)(\Delta z)^2 + \cdots O(\Delta z^4),$$
$$c = c_{(0)} + (\Delta z)^2 c_{(1)} + (\Delta z)^4 c_{(2)} + \cdots,$$
$$\mathscr{W} = \mathscr{W}_{(0)} + (\Delta z)^2 \mathscr{W}_{(1)} + (\Delta z)^4 \mathscr{W}_{(2)} + \cdots. \tag{2.21}$$

Then, the equations grouped in the order of Δz^2 are given by:

$$\left(c_{(0)} - \gamma\mathscr{U}\right)\left(\mathscr{W}''_{(0)} - \mathscr{W}_{(0)}\right) + \gamma\frac{1}{\Delta z}\left[\frac{\mathscr{U}(z+\Delta z) - \mathscr{U}(z)}{\Delta z} - \frac{\mathscr{U}(z) - \mathscr{U}(z-\Delta z)}{\Delta z}\right]\mathscr{W}_{(0)} = 0,$$

$$\begin{aligned}&\left(c_{(0)} - \gamma\mathscr{U}\right)\left(\mathscr{W}''_{(1)} - \mathscr{W}_{(1)}\right) + c_{(1)}\left(\mathscr{W}''_{(0)} - \mathscr{W}_{(0)}\right),\\ &\quad + \gamma\frac{1}{\Delta z}\left[\frac{\mathscr{U}(z+\Delta z) - \mathscr{U}(z)}{\Delta z} - \frac{\mathscr{U}(z) - \mathscr{U}(z-\Delta z)}{\Delta z}\right]\mathscr{W}_{(1)}\\ &= -\tfrac{1}{12}\mathscr{U}''''(z)\mathscr{W}_{(0)},\\ &\quad \ldots.\end{aligned} \tag{2.22}$$

The zero-order equation is the piecewise-linear approximation. Therefore, the approximation accuracy is proportional to the square of the layer thickness, $O(\Delta z^2)$, or in dimensional z-axis $O[(k\Delta z)^2]$.

The results of this section can be summarized as: $\forall c \in \mathscr{C}$ and the corresponding eigenfunction $\mathscr{W}(z,c) \in \mathscr{F}$; there is a corresponding eigenvalue and eigenfunction of the piecewise-linear system, which lies in the neighbourhood of $O(\Delta z^2)$. The reverse is not necessarily true, as we shall see in the next section.

3. Dispersion relation

Assuming that $W(z \leqslant z_n)$ and $W'(z \leqslant z_n)$ are known, the equations for constants $W(z_i) = W_i$, $i = 0, \ldots, n$ can be written more concisely in a matrix form as:

$$[B]W = 0, \tag{3.1}$$

where $[B]$ is an $(n+1)\times(n+1)$ tridiagonal Jacobi matrix (see the Appendix). The eigenvalue or wave speed, c, can be found from the dispersion relation of the corresponding surface wave:

$$\det[B]=0. \tag{3.2}$$

This can also be expanded in a three-term recurrence relation as:

$$\left[(c-\gamma U_o)^2+\frac{S}{C}\gamma b_o(c-\gamma U_o)-\frac{S}{C}\right]W_o=\left[\frac{1}{C}(c-\gamma U_o)^2\right]W_1, \tag{3.3a}$$

$$W_{i+1}=2CW_i-\frac{S\gamma(b_{i-1}-b_i)}{(c-\gamma U_i)}W_i-W_{i-1}, \tag{3.3b}$$

$$W_{n-1}=\left[S\tanh(kH-kD)+C-\frac{\gamma S(b_{n-1}-U_n')}{(c-\gamma U_n)}\right]W_n, \tag{3.3c}$$

where C and S denote $\cosh(\Delta z)$ and $\sinh(\Delta z)$, respectively. Naturally, a simpler expression of the dispersion relation can be found for small values of n. Using an appropriate choice of n, D and H, some examples are given in the Appendix, including the dispersion relations for shallow-water linear velocity (Biesel 1950; Peregrine 1976; Kirby & Chen 1989), deep-water single constant shear layer (Stern & Adam 1973) and two linear velocity layers (Longuet-Higgins 1998).

As an example of continuous velocity profiles for comparison, we choose the finite depth $\mathscr{U}=\mathscr{U}_o\cos(\pi z/2D)$ profile. The profile, together with other surface velocity profiles used in this paper, is shown in figure 1. The analytic solution can be found for the case of $c=0$, i.e. phase-stationary waves that travel against the current. The wave vertical-velocity has three forms depending on the wavelength relative to the depth:

$$\left(\frac{\pi}{2Dk}\right)^2<1\Rightarrow\mathscr{W}=A\sinh\left(\sqrt{1-\left(\frac{\pi}{2Dk}\right)^2}\,k(D+z)\right), \tag{3.4a}$$

$$\left(\frac{\pi}{2Dk}\right)^2>1\Rightarrow\mathscr{W}=A\sin\left(k(D+z)\sqrt{\left(\frac{\pi}{2Dk}\right)^2-1}\right), \tag{3.4b}$$

$$\left(\frac{\pi}{2Dk}\right)^2=1\Rightarrow\mathscr{W}=A(D+z). \tag{3.4c}$$

The corresponding dispersion relations are:

$$Fr^2=\frac{1}{Dk\sqrt{1-(\pi/2Dk)^2}}\tanh\left(Dk\sqrt{1-\left(\frac{\pi}{2Dk}\right)^2}\right)=\frac{\tanh\kappa_1}{\kappa_1}, \tag{3.5a}$$

$$Fr^2=\frac{1}{Dk\sqrt{(\pi/2Dk)^2-1}}\tan\left(Dk\sqrt{\left(\frac{\pi}{2Dk}\right)^2-1}\right)=\frac{\tan\kappa_2}{\kappa_2}, \tag{3.5b}$$

$$Fr^2=\frac{(\mathscr{U}_o)^2}{gD}=1. \tag{3.5c}$$

Our calculation by piecewise-linear approximation matches the analytic form above very well, as shown in figure 2. The calculation accuracy increases as the number of layers, n, increases. After $n>10$, the solutions become fairly accurate and the numerical truncation error also becomes a factor.

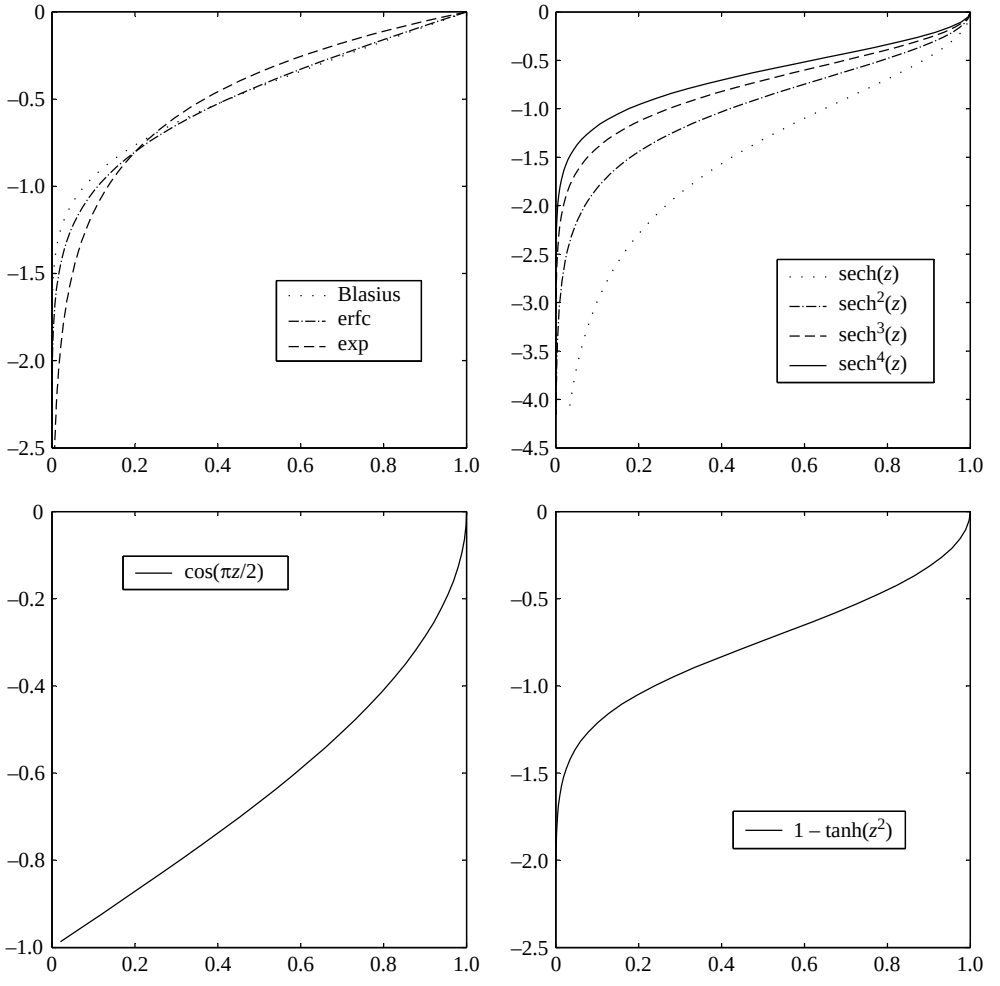

FIGURE 1. Various boundary-layer velocity profiles used in this paper. The vertical axis is for water depth with mean surface at 0, and the horizontal axis is for the normalized current velocity.

Let us look further at some general properties of the dispersion relation defined by (3.2). Figure 3 shows the logarithm of the absolute value of det$[B]$ plotted as a function of wave speed c for a sech$^2(z)$ surface-shear profile. The choice of a particular surface-shear profile is not critical here. The wave speeds of linear waves in still water are $c = \pm 1$ (normalized) correspondingly. The real roots of the dispersion relation are at the dips in the figure where the determinant changes sign. The shear current is in the range of $[0, 0.5]$. Normally, there are two roots of the dispersion relation that are associated with neutral surface waves, c_1, and c_2. One travels with and the other travels against the current. In the figure, $c_1 > 1$ and c_2 is between -1 and 0. The other roots are those modes whose phase speeds equal the current speed at some depth, $c - \gamma U(z_c) = 0$. Without introducing an additional viscous balance term or nonlinear term to the governing equation, if z_c is in the linear part of velocity profile, $U(z)$, $z \neq z_i$, then the equation of the layer that includes z_c becomes:

$$W'' + W = a\delta(z_c), \quad z_{i-1} > z_c > z_i. \tag{3.6}$$

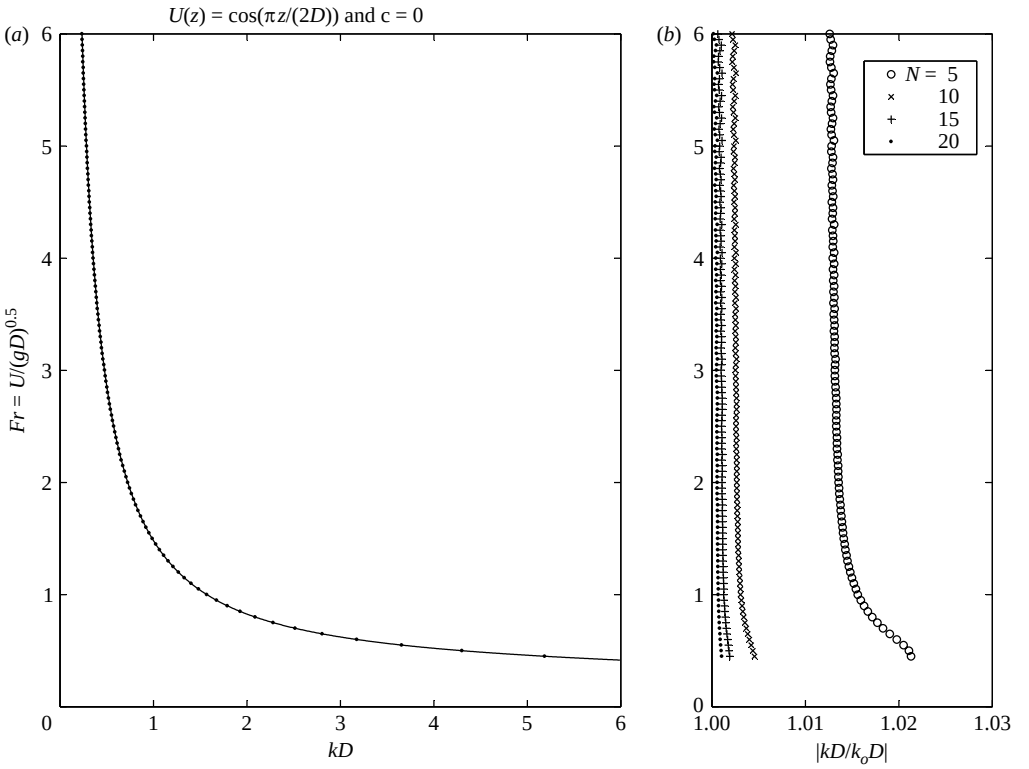

FIGURE 2. (*a*) A comparison between the analytic solution (solid line) and the PLA 20-layer approximation (dots). Here, the wavenumber of stationary waves ($c = 0$) on a surface shear with cosine vertical profile is plotted against the Froude number. (*b*) To demonstrate the calculation accuracy of dispersion relation (3.5) as the number of layers increases, the ratios of wavenumber k calculated by PLA and wavenumber k_o by (3.5) are shown for given Froude numbers.

The possible solutions do not require that $W(z_c) = 0$.

When z_c is at a layer interface, $z_c = z_i$, from the vorticity jump condition (2.12), either the vertical velocity or vorticity change has to be zero at the interface. First, when there is a vorticity jump between the two interface layers:

$$U'(z_i+) - U'(z_i-) \neq 0 \Rightarrow W(z_i) = 0. \tag{3.7}$$

For normal boundary-layer flows, the only possible modes in this situation are those 'surface-layer solutions' (Peregrine 1976) whose motions are limited within the fluid above the critical layer. If it exists, it has to satisfy the dispersion relation for this class of surface-layer solution:

$$\left[(c-\gamma U_o)^2 + \frac{S}{C}\gamma b_o(c-\gamma U_o) - \frac{S}{C}\right] - \left[\frac{1}{C}(c-\gamma U_o)^2\right]\frac{W_1}{W_o} = 0, \tag{3.8a}$$

$$\frac{W_i}{W_{i-1}} = \frac{1}{2C - \dfrac{S\gamma(b_{i-1}-b_i)}{(c-\gamma U_i)} - \dfrac{W_{i+1}}{W_i}}, \tag{3.8b}$$

$$W_{ic-2} = \left[2C - \frac{\gamma S(b_{ic-2}-b_{ic-1})}{(c-\gamma U_{ic-1})}\right] W_{ic-1}, \tag{3.8c}$$

$$c = U_{ic}. \tag{3.8d}$$

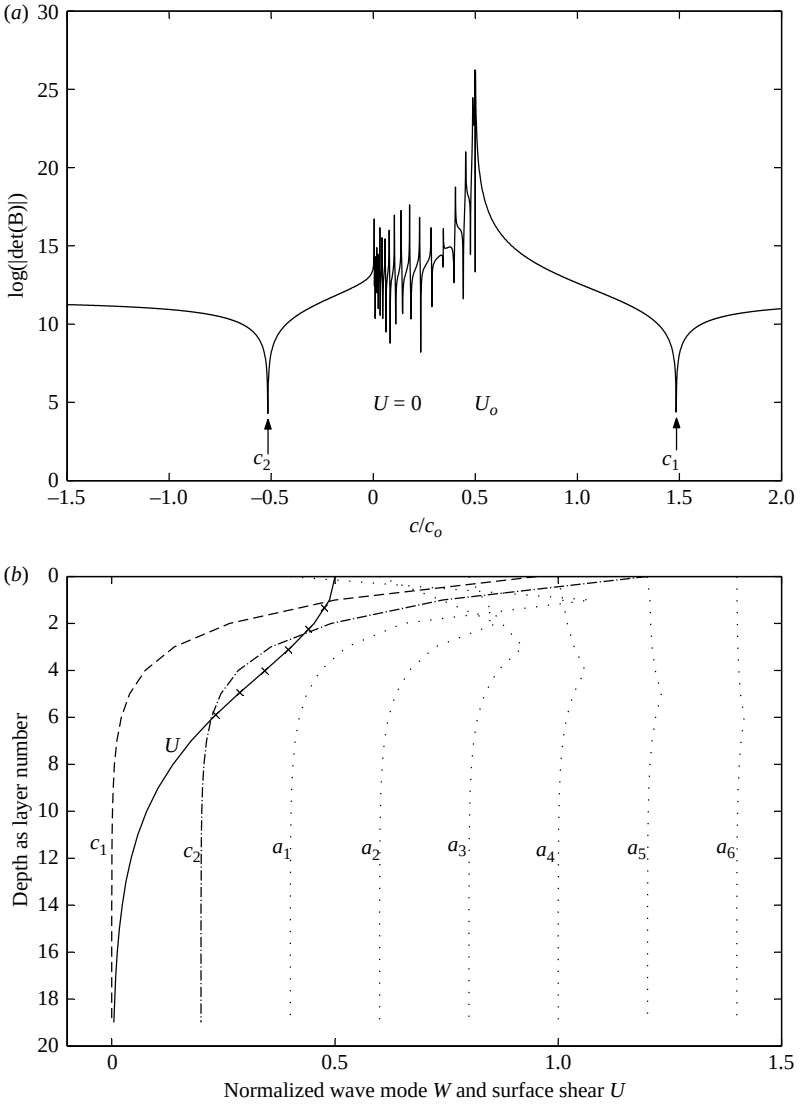

FIGURE 3. (*a*) The logarithm of the absolute value of det[B] is plotted as a function of wave speed c for a sech$^2(z)$ surface-shear profile. The real roots of the dispersion relation are at the dips in the plot. For a given wavenumber k, there are two corresponding waves, c_1 and c_2. They correspond to the waves with the speeds of $\pm c_o$, for zero current. When $U_{max}/c_o > 1$, c_2 can be in the range of $[U_{min}, U_{max}]/c_o$, and becomes unstable. (*b*) Profiles of vertical velocity amplitude for different modes. The profiles of modes c_1 and c_2 (dashed and dot-dashed curves) are close to e^{kz}, while the profiles of artificial modes (marked as $a_1 - a_6$) have a maximum near the critical point. Only 6 artificial modes are shown with dotted curves. They correspond to the 6 largest eigenvalues and the depth of their critical layers are marked by $\times$ on the surface current profile (the solid curve). Each mode curve is offset horizontally by an increment value of 0.2.

For a constant shear profile, it reduces to (A 1) with $z_{ic} = z_c$ (Peregrine 1976). Correspondingly, the bottom-layer solution (not surface wave solutions) possibly exists if $\mathscr{U}''/(\mathscr{U} - c)$ is not always positive below (Yih 1972).

Secondly, the case of $U'(z_{ic}+) - U'(z_{ic}-) = 0$ at the layer interface is the same as the case where $z_{i-1} > z_c > z_i$. There can be solutions of $W(z_{ic}) \neq 0$. They are similar to the

neutral solutions of continuous velocity profiles where $\mathscr{U}''(z_c)=0$. However, we must be extremely careful when a piecewise-linear profile of many layers is used for the approximation of a continuous velocity profile in the range of $U_{min}\leqslant c\leqslant U_{max}$. More often than not, $U''(z_c)=0$ or $U'(z_{ic}+)-U'(z_{ic}-)=0$, but the second derivative of the corresponding continuous shear flow $\mathscr{U}''(z_c)\neq 0$. The Rayleigh equation is obviously singular at the critical layer unless $\mathscr{W}(z_c)=0$. Therefore, the regular solutions from (3.6) that lead to $\mathscr{W}(z_c)\neq 0$ are not permitted by the continuous system in the case of $\mathscr{U}''(z_c)\neq 0$. Only when the second derivative equals zero does the Reynolds stress become discontinuous at the critical layer where wave phase velocity equals the current speed, and this is necessary for instability to occur. Some neutral solutions arising from a piecewise-linear profile approximation are thus artificial, because in reality $\mathscr{U}''(z_c)\neq 0$.

This can be demonstrated by first taking $\mathscr{U}(z)$ as a simple linear velocity profile. Since $U''(z_c)=0$ is the same as $\mathscr{U}''(z_c)=0$ in this case, it always achieves the same eigenvalues no matter how many layers we use in the calculation. The second example is $\mathscr{U}(z)=\mathrm{sech}^2(z)$, approximated by a 20 piecewise-linear system as shown in figure 3. There are more than 18 artificial modes with eigenvalues of $c_l\in[U_{min}, U_{max}]/c_o$ for the PLA system shown in figure 3(*a*). Some selected profiles of eigenfunctions are also shown in figure 3(*b*). Non-artificial modes are possible only at inflection points where $c_{infl}=0,\ \text{or } 1/3$.

As we will demonstrate in the next section, high accuracy can be achieved if PLA is used correctly. Here, we limit our discussion to the evolution of infinitesimal perturbations in shear flows in terms of wavelike normal modes. When linearly unstable modes exist, they eventually prevail in the solutions to linear and nonlinear initial problems. The piecewise-linear approximation method can be used efficiently with the help of inflection point theory. However, when there are no linear unstable modes, it is still not totally clear how precisely to compare the unstable modes of the piecewise-linear profiles with the solutions of a continuous velocity profile (Shrira & Sazonov 2001).

In general, there is not a one-to-one correspondence between the solutions of the Rayleigh equation for a continuous velocity profile and the solutions of the PLA. The dispersion relation of the PLA is a high-order polynomial equation. The number of PLA eigenvalues can increase rapidly with the number of layers, N. Let C_N be a subspace of the complex numbers that consists of all the eigenvalues of PLA of N layers. The subspace C_N can be extended along the boundaries by a distance D_N of $O(\Delta z^2)$, noted as $C_N\oplus D_N$, so that $\mathscr{C}\subseteq C_N\oplus D_N$. Further, $\mathscr{C}\subseteq S\{N\}$, where $S\{N\}=\cap_{\{N\}}(C_N\oplus D_N)$ is the joint set of $C_N\oplus D_N$ for different values of N. The same is true for eigenfunctions in the functional space.

4. Instabilities of horizontal shear flows with a free surface

The instability of a horizontal shear flow with a free surface has important applications in the study of the surface wakes of ships or near-surface bodies (Dimas & Triantyfallou 1994); of the stability of the crest of a spilling wave breaker (Coakley & Duncan 1997); and of wind-drift currents (Stern & Adam 1973; Morland, Saffman & Yuen 1991). There are only a few cases where an analytic solution can be found; thus, the solutions of realistic surface shear profiles largely depend on elaborate numerical calculations. PLA can be a very efficient and accurate tool for such applications on shear-flow instability.

4.1. *Surface shear flows with* sech *type profiles*

A well-studied case is the linear instability of a shear flow with a continuous velocity profile of the form $\mathscr{U} = \mathscr{U}_o \operatorname{sech}^2(bz)$. The shear flow with this profile was numerically studied by Triantyfallou & Dimas (1989) and Dimas & Triantyfallou (1994), and was found to fit experimental data for the shear flow in the wake of a hydrofoil. For the linear instability analysis, the neutral modes form the stability boundaries. Yih (1972) showed that if $\mathscr{U}(z)$ is a monotonic function of depth, as in most boundary-layer flows, for a neutral surface-wave mode with a speed $c \in (\mathscr{U}_{min}, \mathscr{U}_{max})$, then $c = \mathscr{U}(z_c)$, where z_c is an inflection point of the velocity profile $\mathscr{U}(z)$. For the $\mathscr{U} = \mathscr{U}_o \operatorname{sech}^n(bz)$ family of surface-shear profiles, the inflection points are at $(z = -\infty, c = 0)$, $(z = (1/b)\sinh^{-1}(\sqrt{1/n}), c = \gamma \operatorname{sech}^n[\sinh^{-1}(\sqrt{1/n})])$ and $(z = 0, c = \gamma)$. Knowing the valid eigenvalue for the continuous current profiles, the wavenumber and waveform can be very precisely calculated by the piecewise-linear approximation. To further determine on what side of the neutral curve there is instability and what the growth rate of instability is, we have to know the stability characteristics in the neighbourhood of the curve, which can be achieved by a variational approximation or a perturbation of the known neutral solution (Miles 1957, 2001; Engevik 2000).

In figure 4, the linear stability diagram for surface gravity waves is shown for the current profiles $\mathscr{U} = \mathscr{U}_o \operatorname{sech}^n(bz)$. For $n = 2$, the analytic solutions have been found (Engevik 2000). Our calculation resulting from piecewise-linear approximation matches the analytic solution accurately. In the figure, the Froude number is defined as $Fr = \mathscr{U}_o/\sqrt{gD}$, $D = b^{-1}$, the same as that chosen by Engevik (2000). The curves (*a*) and (*c*) are the loci of the neutral solution with velocity $c = \gamma \operatorname{sech}^n[\sinh^{-1}(\sqrt{1/n})]$, and curve (*b*) is the locus of the neutral solution with $c = 0$. The shaded regions are the unstable regions. There are two distinct regions of unstable modes for a given Froude number for this entire family of velocity profiles, previously referred to as branches I and II by Triantyfallou & Dimas (1989) for the case of $n = 2$. The low-wavenumber branch I widens as the Froude number decreases. There are no wavenumber components of branch II when $Fr = 0$, and the wavenumber region becomes very wide around $Fr = 1$, then narrows, bounded at both the high- and low-wavenumber sides. We have calculated the profiles up to $n = 10$. Branches I and II never merge. As n increases, or the profiles become steeper (figure 1), the curve of locus (*a*) moves towards a high wavenumber for all Froude numbers, while the curve (*c*) moves towards a high wavenumber only at high Froude numbers. At high Froude numbers ($Fr > 3$), branch I shrinks to a very narrow region $kD \ll 1$.

By mapping from the wavenumber for gravity waves $k_g D$ to the wavenumber for gravity–capillary waves $k_c D$ according to the relation $k_g D = k_c D/B(k_c D) = k_c D/(1 + (T/gD^2)k_c D)$, the surface tension effect for very short waves can easily be included. As shown in figure 5, branch II of the high-wavenumber instability region is further stretched towards the high-wavenumber end. Branch I is not affected. As noticed in the $n = 2$ case by Engevik (2000), there are minimum points on the curves of the boundaries of branch II for all n. Unlike the long gravity waves, the short gravity–capillary waves are stable below a certain Froude number for this family of velocity profiles.

4.2. *Surface shear flows with tanh type profiles*

Another type of velocity profile is:

$$\mathscr{U} = \mathscr{U}_o(1 - \tanh(b(y/D)^2),$$

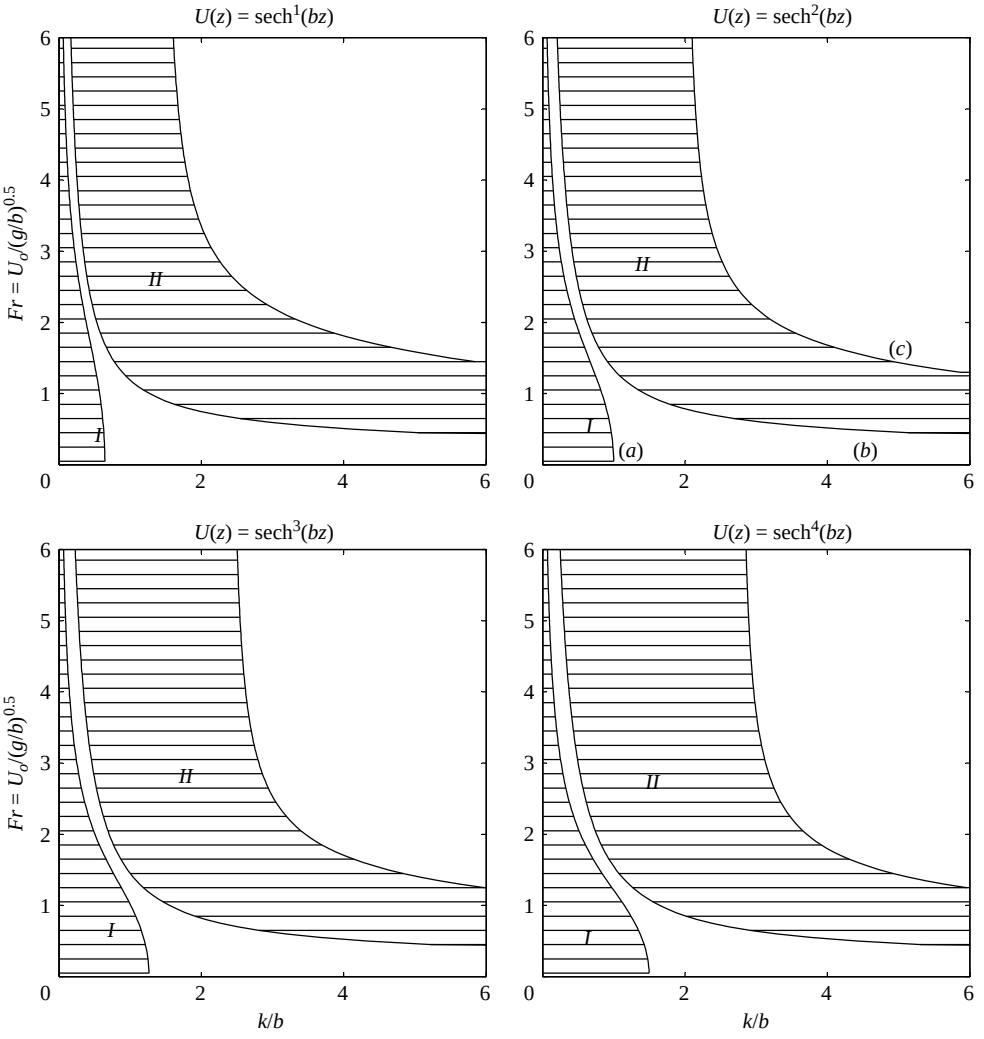

FIGURE 4. Stability diagrams calculated from PLA for the velocity profile $\mathscr{U} = \mathscr{U}_o \operatorname{sech}^n(bz)$ family with no surface tension, i.e. $T = 0$. The two shaded regions are the unstable regions, branch I at low wavenumbers and branch II at higher wavenumbers. The curves (a) and (c) are the loci of the neutral solutions with velocity $c_s = \gamma \operatorname{sech}^n[\sinh^{-1}(\sqrt{1/n})]$, and the curve ($b$) is the locus of the neutral solutions with $c_s = 0$. In the PLA calculations, non-dimensional Δz is chosen as $1/20$.

representing the surface shear-flow in the second wave trough behind a steady breaking wave (Duncan & Dimas 1996). This tanh profile (figure 1) has an inflection point in the middle, the same as the sech profile family. A difference is that the top velocity layer is thicker than the sech profile. An interesting feature of its linear stability diagram for surface gravity waves (figure 6) is that branches I and II overlap in space, in sharp contrast to that of the sech profile. The two unstable regions do not necessarily merge into one branch, although they cross through each other. To the best of our knowledge, there are currently no other published reports on linear stability diagrams for the tanh profile.

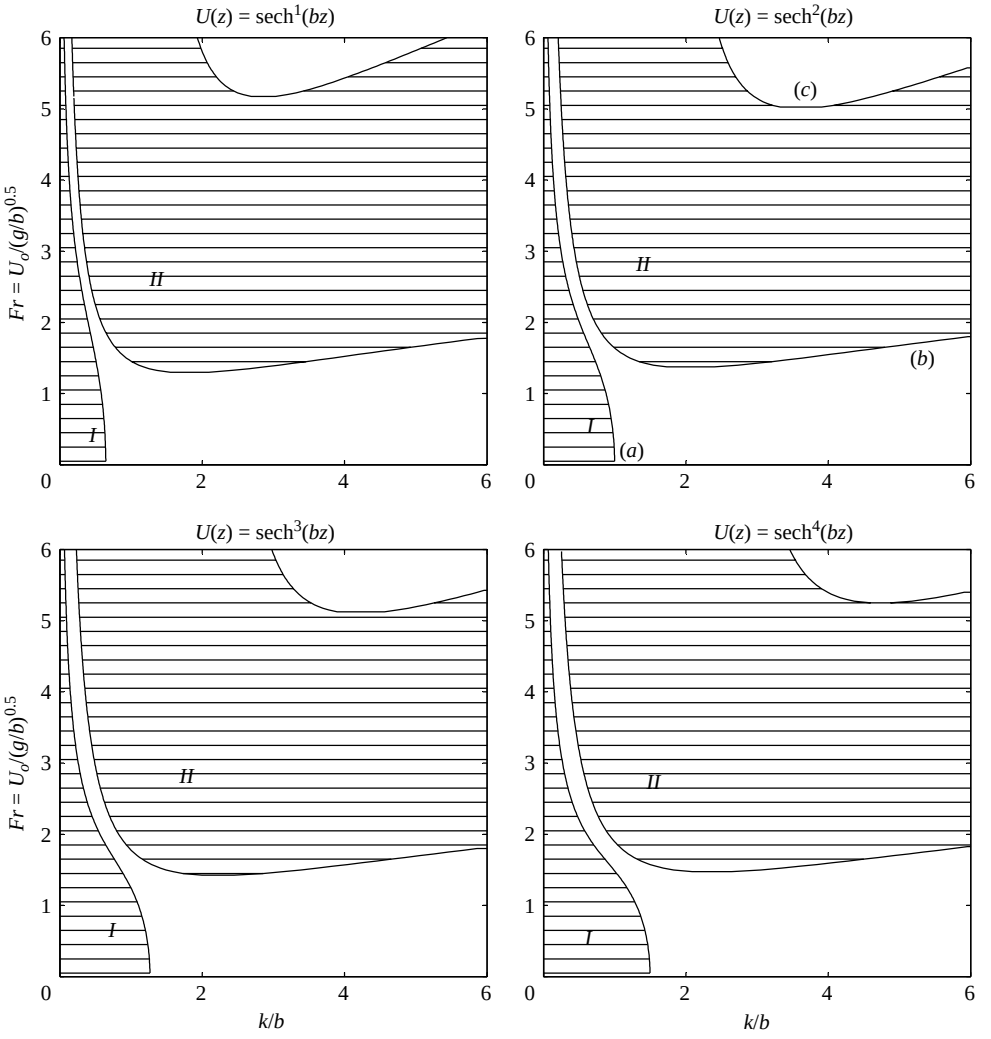

FIGURE 5. Same as figure 4 with surface tension present, $T/gD^2 = 0.5$. In the PLA calculations, non-dimensional Δz is chosen as $1/20$.

4.3. *Surface shear flows with profiles without inflection point in the middle*

In a study on possible mechanisms for the generation of short gravity–capillary waves by wind drift currents, various boundary-layer velocity profiles are used by Morland *et al.* (1991), including exponential and error function profiles. These types of velocity profile have non-zero slope at the surface and there is no inflection point in the middle of the profiles. The neutral mode exists only at $c = 0$ and there is an analytic solution for the exponential profile. Figure 7 shows the neutral stability curves for the exponential, error function and Blasius function from PLA calculation. The neutral stability of the Blasius profile has not previously been reported. They are plotted in the $(\lambda/\Delta, c_o/\mathscr{U}_o)$-plane based on numerical results shown by Morland *et al.* (1991). Here, Δ is a vertical normalization scale defined as:

$$\Delta = \frac{2}{\mathscr{U}_o} \int_{-\infty}^{0} \mathscr{U}(z)\, \mathrm{d}z.$$

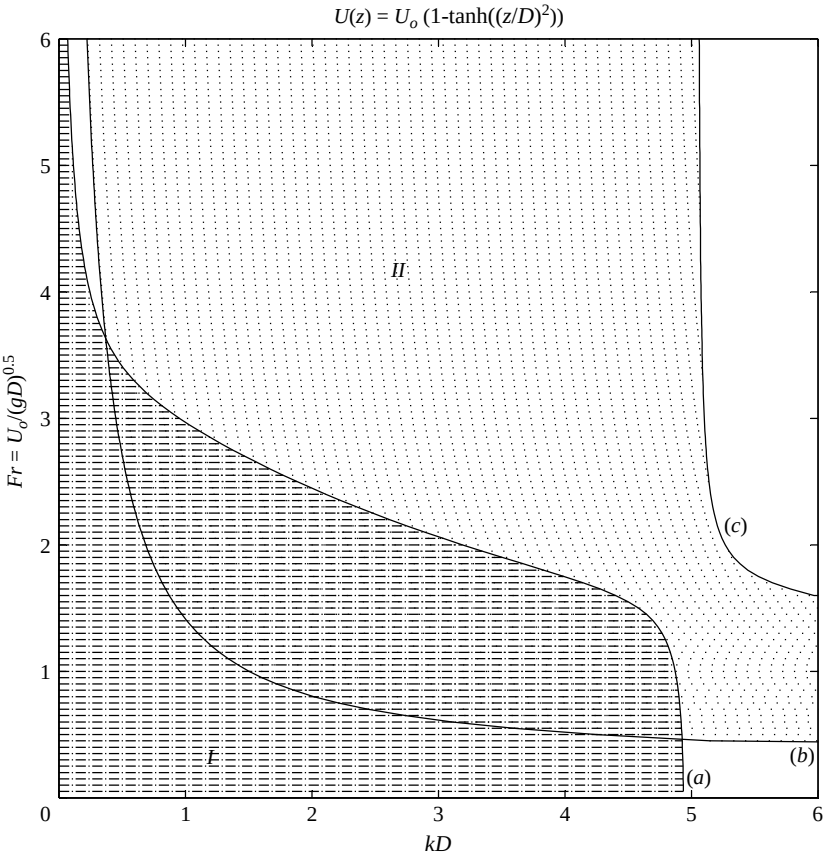

FIGURE 6. Stability diagrams calculated from PLA for the velocity profile $\mathscr{U} = \mathscr{U}_o(1 - \tanh(b(y/D)^2)$. No surface tension, i.e. $T = 0$. The two shaded regions are the unstable regions, branch I at low wavenumbers and branch II at higher wavenumbers. The curves (*a*) and (*c*) are the loci of the neutral solutions associated with the inflection point $0.5218^{1/2}$, and the curve (*b*) is the locus of the neutral solutions with $c_s = 0$. There is an overlap region between branches I and II. In the PLA calculations, non-dimensional Δz is chosen as 1/20.

λ/Δ is proportional to $(kD)^{-1}$ and $c_o/\mathscr{U}_o$ relates to the Froude number by $c_o/\mathscr{U}_o = (1/Fr)(1+B(kD)/kD)$. Among these profiles, the error function has the largest unstable region and the Blasius profile has the smallest. It is more stable for short waves than longer waves. All waves are stable when the surface flow is slower than the intrinsic linear wave speed. There must be a strong surface drift for short waves to become linearly unstable. Also, these possible unstable waves have to propagate into the drift currents and wind. For waves propagating with the wind or drift – that is, c_1 in figure 3 – the effect of surface shear is mostly to increase their propagation speeds, as we will discuss in the following section.

5. Propagation of short surface waves under influence of wind drift

We will now consider short waves with phase speeds that are not in the range of $(U_{\min}, U_{\max})$, i.e. those that are linearly stable. The linear mechanism that modifies the propagation of surface waves by currents is well understood. However, the applications to short waves on surface currents are so far very limited. First of all,

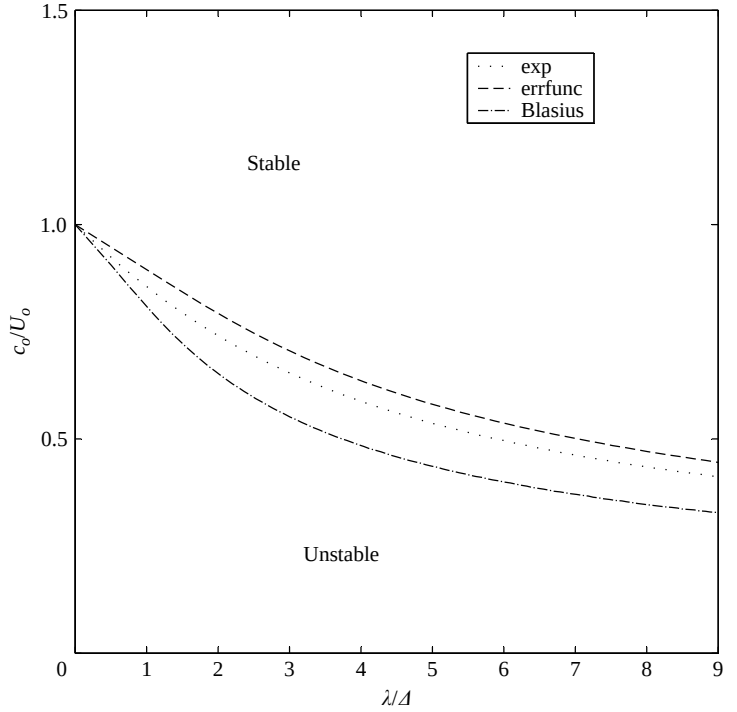

FIGURE 7. Marginal stability curves calculated by PLA for three different boundary-layer profiles. The parameters are chosen as in Morland *et al.* (1991) for direct comparison. An exact fit is found between two methods for the exponential (short dashed) and error function (long dashed) profiles. The dot-dashed curve is for the Blasius profile, which is more stable than the other two. 60 layers are used in the PLA calculations.

it is not an easy task to measure the profiles of the surface currents in most cases. Secondly, our calculations on propagation speed have relied heavily on perturbation approximations, which may no longer converge. By the linear-piecewise approximation developed above, we are able to calculate the wave propagation speed accurately for any given realistic surface flow profile, and thus are able to evaluate the availability of perturbation approximations.

Without any approximation, an implicit form of the dispersion relation can be found (Miles 2001), through multiplying $\mathscr{W}$ to the governing equation (1.1), integrating over the depth, integrating by parts and applying the surface and bottom boundary conditions:

$$\mathscr{U}_o'(\mathscr{U}_o - c) + kc_o^2 = \kappa(\mathscr{U}_o - c)^2, \tag{5.1}$$

where

$$\kappa = \int_{-\infty}^{0} \mathrm{d}z \left[\left(\frac{\mathscr{W}'}{\mathscr{W}(0)} \right)^2 + \left(\frac{\mathscr{W}}{\mathscr{W}(0)} \right)^2 k^2 + \left(\frac{\mathscr{W}}{\mathscr{W}(0)} \right)^2 \left(\frac{\mathscr{U}''}{\mathscr{U} - c} \right) \right]. \tag{5.2}$$

Equation (5.1) is quadratic in c, hence

$$c = U_o - \frac{k}{\kappa}\frac{\mathscr{U}_o'}{2k} \pm \sqrt{\frac{k}{\kappa}c_o^2 + \left(\frac{k}{\kappa}\frac{\mathscr{U}_o'}{2k} \right)^2} = \mathscr{U}_o - c_o \frac{k}{\kappa} \left[\frac{\mathscr{U}_o'}{2c_o k} \pm \sqrt{\frac{\kappa}{k} + \left(\frac{\mathscr{U}_o'}{2c_o k} \right)^2} \right], \tag{5.3}$$

with a parameter $\kappa(c, \mathscr{W}(\cdot), \mathscr{U}(\cdot)) \neq 0$ to be determined, or in the non-dimensional form:

$$c = +\gamma \mathscr{U}_o - \frac{k}{\kappa}\frac{\gamma \mathscr{U}'_o}{2sk} \pm \sqrt{-\frac{k}{\kappa} + \left(\frac{k}{\kappa}\frac{\gamma \mathscr{U}'_o}{2sk}\right)^2}. \tag{5.4}$$

Without solving for $\mathscr{W}$, we propose here that κ may be estimated by letting $\mathscr{W} \sim \mathrm{e}^{kz}$ in an approximation of the first order for deep-water waves, then

$$\kappa_o \sim k + \frac{1}{2}\int_{-\infty}^{0} \mathrm{d}z \left(\frac{\mathrm{e}^{2kz}\mathscr{U}''}{\mathscr{U} - c_{(o)}}\right), \tag{5.5}$$

where $c_{(o)} = \mathscr{U}_o - \mathscr{U}'_o/2k \pm \sqrt{c_o^2 + (\mathscr{U}'_o/2k)^2}$ for short waves ($\varepsilon \ll 0$, Shrira 1993) and $c_{(o)} = c_o - \mathscr{U}$ for long waves ($\gamma \ll 0$, Stewart & Joy 1974). In the limit of long waves,

$$\kappa_o = k - \frac{1}{c_o}\left(\mathscr{U}'_o - 2k\mathscr{U}_o + 4k^2\int_{-\infty}^{0} \mathscr{U}\mathrm{e}^{2kz}\,\mathrm{d}z\right). \tag{5.6}$$

The last term in the parentheses is of the order of γ and becomes comparable to wave number k as the wavelength increases. This would lead to $k/\kappa \to \infty$, a divergence that can be avoided by including the next order of wave solution, for example,

$$\mathscr{W} \sim \mathrm{e}^{kz} + \gamma \mathrm{e}^{-kz}\int_{-\infty}^{z} \mathscr{U}'(y)\mathrm{e}^{2ky}\,\mathrm{d}y$$

(Stewart & Joy 1974).

For the case of short waves on wind-drift shear, various boundary-layer profiles are tested against PLA calculations to check the availability of different perturbation approximations given by Stewart & Joy (1974), by Shrira (1993), and by combination of (5.3) and (5.5) proposed here. Only the results of Blasius and sech^2 profiles are shown here in figures 8 to 11, in order of increasing Froude numbers. Only waves propagating in the wind direction are shown here, and they are in the range of 1 cm to 50 cm. The current speeds at surface $\mathscr{U}_o$ and shear depth D are chosen to cover a realistic wind drift range according to the well-known laboratory measurements by Wu (1975). Figure 9, with a Froude number of 0.34, matches the measured profile at a wind speed of about $5\,\mathrm{m\,s^{-1}}$, and figure 10 corresponds to a wind speed of about $12\,\mathrm{m\,s^{-1}}$ ($Fr = 0.43$). Figure 8 ($Fr = 0.21$) and figure 11 ($Fr = 0.68$) represent the lower and higher Froude numbers of the extended shear-flow range. In general, Stewart & Joy's approximation holds well for-long waves, while Shrira's approximation (first-order only in his (4.10)) is good for high wavenumbers. For the $\mathrm{sech}^2(z)$ profile, Shrira's approximation has a large discrepancy owing to $\mathscr{U}'_o = 0$. To include more depth-averaged effects for this case, it is necessary to use the higher orders from the Shrira series expansion, which has proved to be convergent. To improve the fit in the wavelength range from middle to short waves without using higher-order series, we let $\mathscr{W} \sim \mathrm{e}^{kz}$ and $c_{(o)} = \mathscr{U}_o - \mathscr{U}'_o/2k \pm \sqrt{c_o^2 + (\mathscr{U}'_o/2k)^2}$ to form an approximation to (5.3), as shown in the thin dotted curves. The new approximation works very well into the range where the long-wave approximation holds. The abrupt departure at low wavenumbers is due to $\kappa \to 0$ and can be avoided by introducing the next-order correction to $\mathscr{W}$.

6. Comments

This study is in part inspired by many questions about the scope of validity of the PLA method, such as: 'Why and when does this method work? How many breaks

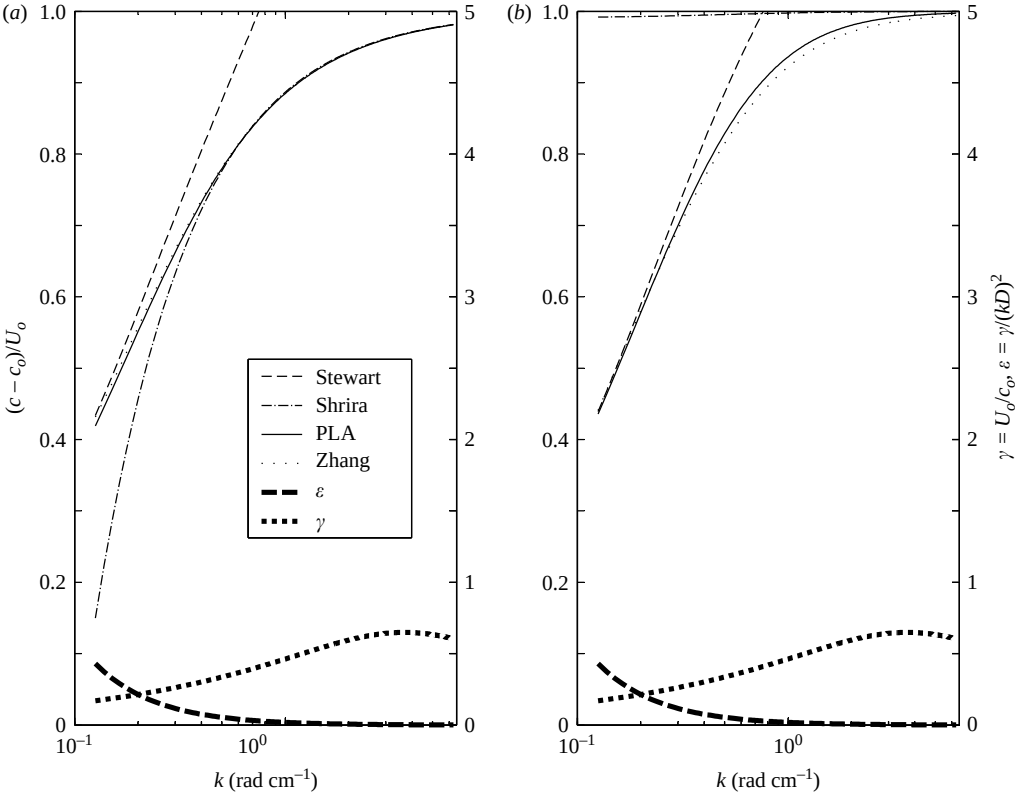

FIGURE 8. Comparison of various approximation schemes. Froude number = 0.21 of weak shear (D = 5 cm and U_o = 15 cm s^{-1}). (*a*) The Blasius velocity profile $Fr = 0.21$ and (*b*) the sech$^2(z)$ velocity profile, $Fr = 0.21$. The thick long and short dashed curves are for non-dimensional scaling constants, ε and γ, respectively, and the scale axis is on the right-hand side. The thin and solid black curve is the calculation using the PLA method, and is used here for reference purposes. The other thin curves represent the different first-order approximations, the dashed thin curves for Stewart & Joy (1974), the dot-dashed curves for Shrira (1993), and the dotted curves for this paper. The surface waves here are in the range of 1 cm to 50 cm.

should be taken? When is the solution structurally stable with respect to the profile smoothing? How many modes do really exist in the original smooth profile flow, if the number of modes in its piecewise linear approximation is equal to the number of breaks specified by the order of the approximation?' (Quotations from Shrira & Sazonov 2001). We have proved the rate of convergence of PLA for solving the Rayleigh equation, which addresses most of the above questions, and looked at the problems of initial instability and propagation speed of short waves on wind drift. The surface boundary conditions are linearized for small-amplitude waves. However, for weakly nonlinear waves, the case for most ocean waves, a higher-order perturbation in wave slope can correspondingly be incorporated into the governing equations solvable by PLA (e.g. Gertsenshtein *et al.* 1988). This will introduce a small correction in the power of the wave slope to the solutions, especially for calculating the propagation speed of waves. Also, surface shears are assumed to be steady and homogeneous, and this corresponds to spatial and temporal averaged ocean surface-currents, e.g. Stokes, and wind drift under steady wind.

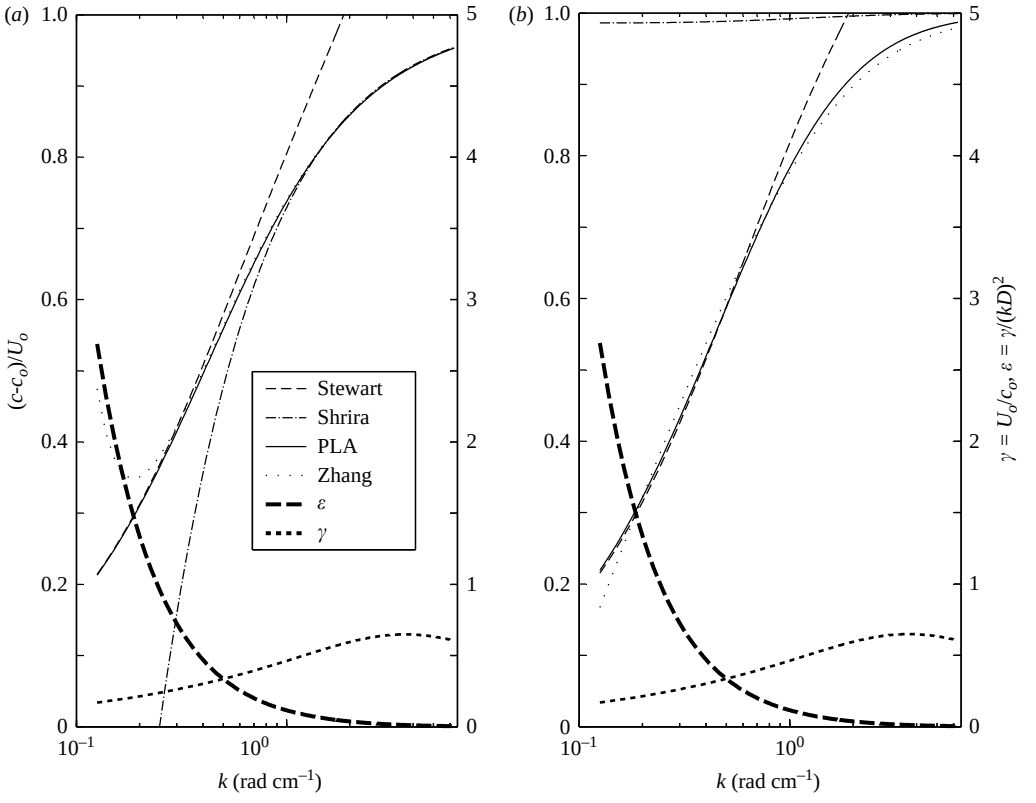

FIGURE 9. Same as figure 8: a comparison of various approximation schemes. Froude number = 0.34 of low wind-speed simulation ($D = 2$ cm and $U_o = 15$ cm s^{-1}). With a smaller shear-layer depth as compared to figure 8, there is less departure from wave speed in still water for longer waves. ε increases quickly towards the long waves, which violates the condition for the Shrira series to converge.

It has been shown (Gertsenshtein 1970) that the Rayleigh equation with homogeneous boundary conditions of the form $\mathscr{W}|_{z=0} = \mathscr{W}|_{z=-H} = 0$ (no flux plane-parallel flow) can be expressed as a bounded linear operator L in the Hilbert vector space as well as a linear operator L_N for the corresponding PLA equation. The approximated eigenvalues from the PLA converge to the real eigenvalues, by giving $\|L - L_N\| \to 0$. With a different approach, our new theory of rate of convergence has several important advantages over Gertsenshtein's convergence theory. (i) There is no more limitation on the type of boundary conditions. (ii) The rate of convergence is given as $O(\Delta z^2)$. (iii) It is recognized that there are artificial modes from PLA which do not belong to the modes of the equation with the continuous velocity profile, i.e. $\|L - L_N\| \to 0$ given by Gertsenshtein (1970) is not always valid.

In order to prove the rate of convergence of PLA, higher-order terms in a power series of Δz have to be introduced. Although the high-order contribution to the numerical value of the total PLA solution is insignificant when the layer thickness approaches zero, the high-order corrections to the vorticity jumping condition are critical in maintaining consistency between the continuous system and the piecewise-linear system. The significance of the correction may need to be investigated further. There are three terms in the Rayleigh instability equation. In a PLA system, the

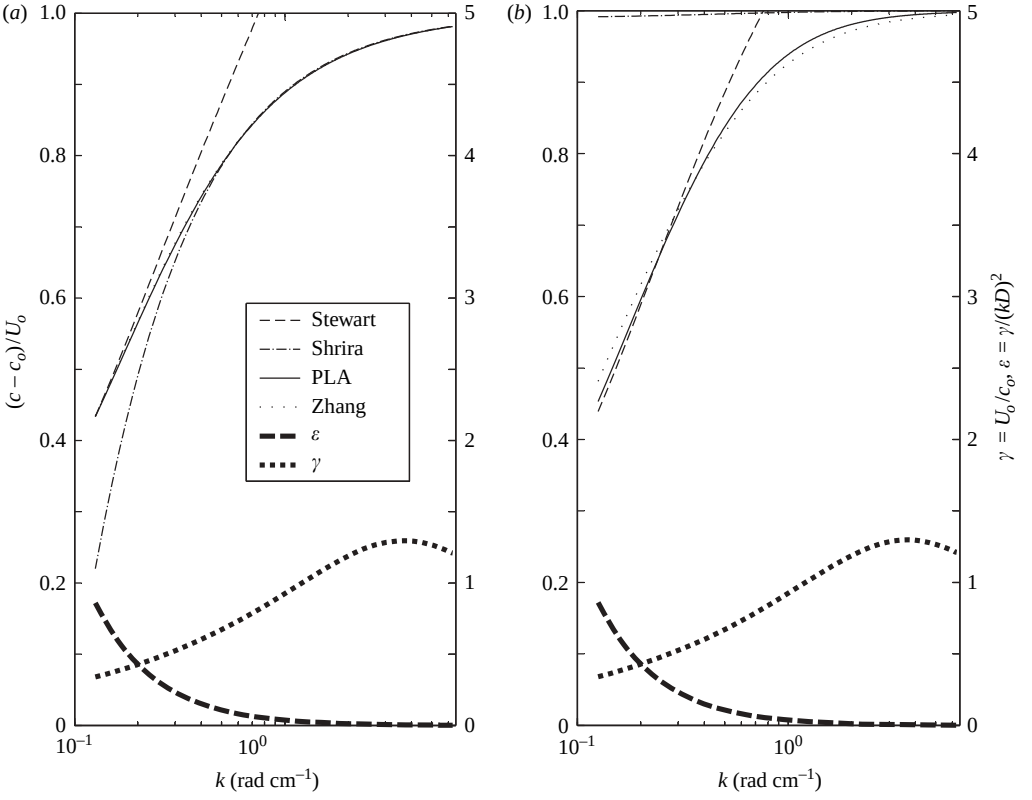

FIGURE 10. Same as figure 8: a comparison of various approximation schemes. Froude number = 0.43 of high wind speed ($D = 4$ cm and $U_o = 30$ cm s^{-1}). γ becomes large as U_o is comparible to the wave speed in still water for most of the waves, violating the validity condition for Stewart expansion.

balances among these three terms are separated into two: $(c - \gamma\mathscr{U})(W'' + W) = 0$ within each of the constant vorticity layers, and $(c - \gamma\mathscr{U})W'' + \gamma\mathscr{U}''W = 0$ at layer interfaces. This is similar to the treatment of a flow system by contour dynamics (Pullin 1991). The drawback in dynamics is that only concentrated vorticity is allowed (Kelvin–Helmholtz model), rather than a real distributed vorticity (Miles 1957).

Despite these limitations, PLA can be a very efficient and accurate tool for calculating shear-flow instability. It is shown that a complete picture of the regimes of unstable modes of different boundary-layer velocity profiles can be achieved very easily and accurately by PLA, whereas they would otherwise have to be handled by complicated numerical schemes. Branches I and II of the instability modes associated with the inflection points of the flow can overlap for tanh-type velocity profiles, but do not overlap for the $\mathscr{U} = \mathscr{U}_o \operatorname{sech}^n(bz)$ velocity profile family, even when n is as large as 10. It is not likely that branches I and II will merge into one branch for the tanh profile, judging from an intuitive requirement of smooth three-dimensional topography for eigenvalue $c = c_{real} + \mathrm{i}c_{image}$ and the calculated marginal modes that form the boundary of the unstable branches. However, for a two-layer model, the two branches can merge, as shown by Longuet-Higgins (1998).

A PLA system may admit additional eigenmodes that do not belong to the corresponding continuous velocity system. Although the accuracy increases with the number of flow layers, the artificial modes can also increase quickly within the range of

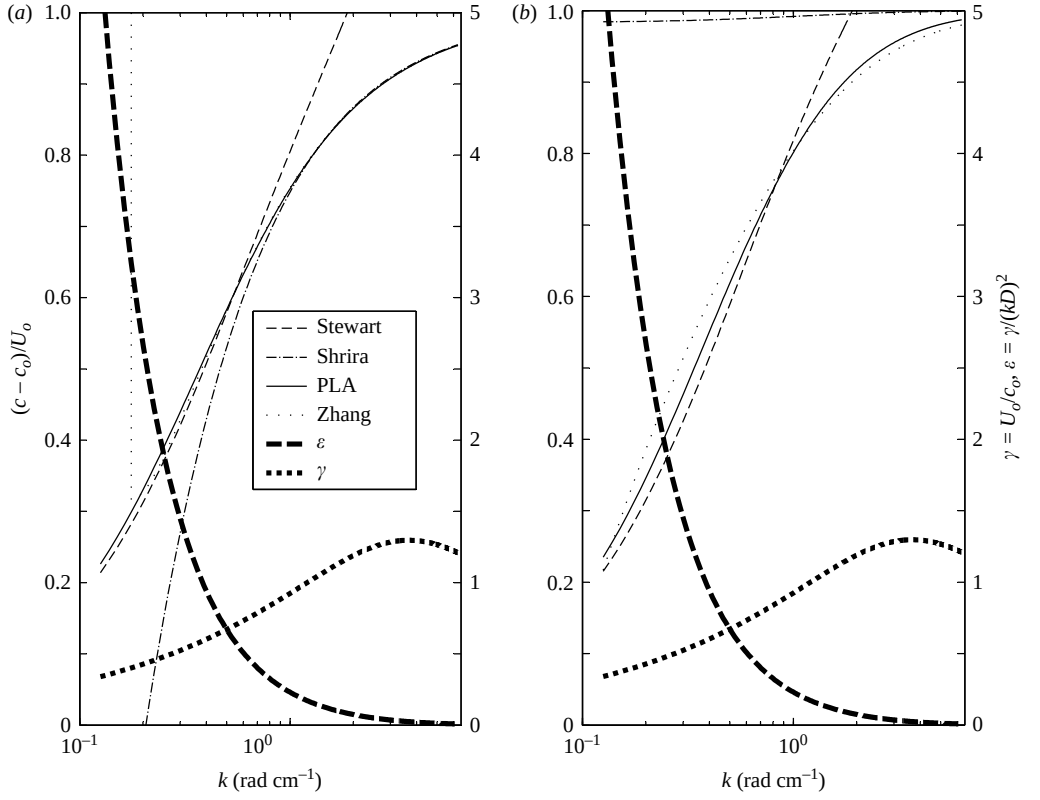

FIGURE 11. Same as figure 8: a comparison of various approximation schemes. Froude number = 0.68 of strong surface shear ($D = 2$ cm and $U_o = 30$ cm s^{-1}). For a small shear layer depth, the low wavenumber waves are less affected by the shear. Here both γ and ε are large in the opposite wavenumber ranges.

$c \in (0, U_o)$. Caution must be used when applying PLA in the range of $c \in (0, U_o)$. It was noted by Shrira & Sazonov (2001) that the phase velocity of every mode in a PLA system varies gradually within the limits of velocities of the particular layer ($[U_{n-1}, U_n]$). This is a typical property of the artificial modes, since the PLA systems set $U'' = 0$ within each interval of $[U_{n-1}, U_n]$, which often violates the original profile $\mathscr{U}'' \neq 0$. One quick way to avoid the artificial modes is by selecting modes using *a priori* knowledge, such as the inflection theory for boundary types of flow. Inflection theory for surface boundary-layer flows (Yih 1972) shows that there is no critical layer at $c = \mathscr{U}$ when $\mathscr{U}'' \neq 0$, which can be used to check the validity of the eigenvalues derived from PLA calculation. For the linear instability of a more complex shear flow system, we might be able to eliminate some artificial modes by cleverly applying the property from the rate of convergence theory that $\mathscr{C} \subseteq S\{N\}$, where $S\{N\} = \cap_{\{N\}}(C_N \oplus D_N)$. Increasing N will increase C_N but decrease D_N, thus changing the shape of $C_N \oplus D_N$. The union of $C_N \oplus D_N$ sets should preserve $\mathscr{C}$. Blindly increasing N may not be the best way to solve the problem. The technical detail is beyond the scope of this paper.

From (5.4), the condition in which c becomes complex is either $\mathrm{Im}(\kappa) \neq 0$, or $\mathrm{Re}(\kappa) < -k(U_o'/2c_o)^2$. Clearly, $\mathrm{Im}(\kappa) \neq 0$ is associated with the critical-layer instability when the integrand in (5.2) contains poles. The path of integration, which formally goes strictly along the real axes, should be chosen, as is common for these types of

hydrodynamic problem, treating the zero order of c as the real limit of the corresponding Laplace index in the Cauchy problem (e.g. Lin 1955; Drazin & Reid 1981). An example for short-wave growth rate is given by Shrira (1993). The second condition $\mathrm{Re}(\kappa) < -k(U_o'/2c_o)^2$ is equivalent to (in non-dimensional form):

$$\frac{\gamma}{s^2}\int_{-\infty}^{0} \mathrm{d}z \left(\frac{W}{W(0)}\right)^2 \left(\frac{U''}{c-\gamma U}\right) > k\frac{\gamma^2}{s^2}\left(\frac{U_o'}{2}\right)^2 + \int_{-\infty}^{0} \mathrm{d}z \left[\frac{1}{s^2}\left(\frac{W'}{W(0)}\right)^2 + \left(\frac{W}{W(0)}\right)^2\right]. \tag{6.1}$$

For long waves, wavenumber $k \to 0$, as does $\gamma = U_o/c_o \to 0$, but the last term remains finite. Therefore, it is unlikely to be satisfied by realistic ocean waves.

PLA is capable of precisely calculating the dispersion relation for stable wave modes for arbitrary velocity profiles, and it is exceptionally important for short waves on wind drift when the conditions for other approximation methods fail. The validity of different approximations can thus be checked. An approximate formula for the dispersion relation is also found here to cover the wavenumber range between long waves covered by the perturbation formula of Stewart & Joy (1974) and short waves covered by the perturbation of Shrira (1993). Two assumptions have been made to extract the approximate dispersion relation from the implicit formula (5.3). Here, we have assumed that the exponential vertical decay for wave motion still holds at the lowest order and that the wave speed can be expanded in a fashion whereby only the lowest order, $c_{(o)}$, is used in the evaluation of the integrand. Our approximate formula fits well for the propagation of short wind waves when it is tested against various kinds of boundary-flow profile in a Froude-number range that covers realistic surface drift. Of course, a better justification, such as the convergence in general, is required.

I am indebted to Dr Guang J. Zhang, Professor Glenn Ierley and Dr Thomas Delmer for going through different versions of the paper during the preparation. I thank Professor Victor Shrira for helpful comments and for bringing the early work on convergence to my attention. The suggestions from anonymous reviewers have improved the final version greatly. This work was financially supported by the National Science Foundation (OCE9811262 and OCE-0118028).

Appendix A

The elements of matrix $[B]$ are:

$$[B] = \begin{bmatrix} \frac{S\gamma b_o}{C}(c-\gamma U_o) + (c-\gamma U_o)^2 - \frac{S}{C} & \frac{1}{C}(c-\gamma U_o)^2 & 0 & 0 & \cdots & 0 \\ 1 & -2C + \frac{S\gamma(b_o-b_1)}{(c-\gamma U_o)} & 1 & 0 & \cdots & 0 \\ 0 & 1 & -2C + \frac{S\gamma(b_1-b_2)}{(c-\gamma U_2)} & 1 & \cdots & 0 \\ \vdots & \vdots & \vdots & \vdots & \ddots & \vdots \\ 0 & 0 & 0 & 0 & \cdots & 1 \\ 0 & 0 & 0 & 0 & \cdots & -(C + S\tanh(kH-kD)) + \frac{S\gamma(b_{n-1}-U_n')}{(c-\gamma U_n)} \end{bmatrix}. \tag{A 1}$$

Its determinant $\det(B)$ is in the general form of a high order $(n+2)$ polynomial of multiple variables $U_o, \ldots, U_m$, including many terms as n increases. However, since the matrix is a tridiagonal Jacobi matrix (used for constructing orthogonal polynomials on the real line), the dispersion relation can be written as a three-term recurrence polynomial, as in (3.3). The simplest case is of a single layer ($\Delta z = kD = s$) of linear velocity. When $H = D$ of finite depth, $W_1 = 0$, the non-dimensional phase speed is reduced to the well-known form (Biesel 1950; Peregrine 1976; Kirby & Chen 1989 for gravity waves) including capillary effect:

$$c = \gamma U_o - \tanh(s)\frac{\gamma b_o}{2} \pm \sqrt{\tanh(s) + \left[\tanh(s)\frac{\gamma b_o}{2}\right]^2}. \tag{A 2}$$

or, in real dimensional form:

$$c = U_o - \tanh(kD)\frac{U_o'}{2k} \pm \sqrt{\left(\frac{g}{k} + Tk\right)\tanh(kD)}\sqrt{1 + \tanh(kD)\frac{[U_o']^2}{4(gk + Tk^3)}}. \tag{A 3}$$

When $H \neq D$, $H = -\infty$, that is, deep-water waves, (3.3) reduces to the same equation as that found by Stern & Adam (1973):

$$Z^3 + \left[\frac{U_o'}{2k}(1 - \mathrm{e}^{-2kD}) + U_o\right] Z^2 - \left\{c_o^2 + \frac{U_o'}{k}\left[-U_o + \frac{U_o'}{2k}(1 - \mathrm{e}^{-2kD})\right]\right\} Z + \left[-U_o + \frac{U_o'}{2k}(1 - \mathrm{e}^{-2kD})\right] c_o^2 = 0, \tag{A 4}$$

where, $Z = (c - \gamma U_o)$, the same parameters as those used by Longuet-Higgins (1998).

For a flow system of two layers with different layer depths of D_1 and D_2, the dispersion relation is:

$$\left[(c - \gamma U_o)^2 + \frac{S_1}{C_1}\gamma b_o(c - \gamma U_o) - \frac{S_1}{C_1}\right]\frac{W_o}{W_1} - \left[\frac{1}{C_1}(c - \gamma U_o)^2\right] = 0, \tag{A 5a}$$

$$\frac{W_o}{W_1 S_1} - \left[\frac{C_1}{S_1} + \frac{C_2}{S_2} - \frac{\gamma(b_o - b_1)}{(c - \gamma U_1)}\right] + \frac{W_2}{W_1 S_2} = 0, \tag{A 5b}$$

$$W_1 = \left[S_2 \tanh(kH - kD_1 - kD_2) + C_2 - \frac{\gamma S_2 b_1}{c}\right] W_2, \tag{A 5c}$$

where C_i and S_i denote $\cosh(kD_i)$ and $\sinh(kD_i)$, respectively. For the finite-depth case when $H = D_1 + D_2$, the dispersion relation is:

$$\left[(c - \gamma U_o)^2 + \frac{S_1}{C_1}\gamma b_o(c - \gamma U_o) - \frac{S_1}{C_1}\right] \times \left\{\left[\frac{C_1}{S_1} + \frac{C_2}{S_2} - \frac{\gamma(b_o - b_1)}{(c - \gamma U_1)}\right] - \frac{c}{S_2[cC_2 - \gamma S_2 b_1]}\right\} - \left[\frac{1}{S_1 C_1}(c - \gamma U_o)^2\right] = 0. \tag{A 6}$$

The dispersion relation for a special case studied by Longuet-Higgins (1998) on surface shear-flow instability in deep water – a constant velocity of the top layer and constant vorticity in the bottom layer – can be found by letting $H = \infty$, $b_o = 0$ and

$U_1 = U_2$ in (A 6):

$$S_1\left[\frac{C_1}{S_1}Z + \frac{C_2}{S_2}Z + \gamma b_1\right]\left[Z^2 - \frac{S_1}{C_1}\right][(S_2 + C_2)(Z+q) - \gamma b_1 S_2]$$
$$- \frac{S_1(Z+q)}{S_2}\left[Z^2 - \frac{S_1}{C_1}\right]Z - \left[\frac{1}{C_1}Z^3\right][(S_2 + C_2)(Z+q) - \gamma b_1 S_2] = 0, \quad \text{(A 7)}$$

which can be shown to be identical to the dispersion relation derived by Longuet-Higgins (1998). Here, $q = \gamma U_o$.

REFERENCES

Abdullah, A. J. 1949 Wave motion at the surface of a current which has an exponential distribution of vorticity. *Ann. N Y Acad. Sci.* **51**, 425–441.

Biesel, F. 1950 Étude théorique de la houle en eau courante. *Houille Blanche* **5**, Numéro Spécial A, 279–285.

Caponi, E. A., Yuen, H. C., Milinazzo, F. A. & Saffman, P. G. 1991 Water wave instability induced by a drift layer. *J. Fluid Mech.* **222**, 297–313.

Coakley, D. & Duncan, J. H. 1997 The flow field in steady breaking waves. *Twenty-First Symp. on Naval Hydrodyn. Trondheim, Norway*, pp. 534–549.

Dimas, A. A. & Triantyfallou, G. S. 1994 Nonlinear interaction of shear flow with a free surface. *J. Fluid Mech.* **260**, 211–246.

Drazin, P. G. & Reid, W. H. 1981 *Hydrodynamic Stability*. Cambridge University Press.

Duncan, J. H. & Dimas, A. A. 1996 Surface ripples due to steady breaking waves. *J. Fluid Mech.* **329**, 309–339.

Engevik, L. 2000 A note on the instabilities of a horizontal shear flow with a free surface. *J. Fluid Mech.* **406**, 337–346.

Fenton, J. D. 1973 Some results for surface gravity waves on shear flows. *J. Inst. Maths. Applics* **1**, 1–20.

Gertsenshtein, S. Ya. 1970 On the convergence of the Rayleigh method. *Sov. Phys. Dokl.* **14**, 746–748.

Gertsenshtein, S. Ya., Romashova, N. B. & Chernyavski, V. M. 1988 On the generation and development of wind waves. *Izv. Akad. Nauk. SSSR Mekh. Zhid. i Gaza* **3**, 163–169.

Gossard, E. E. & Hooke, W. H. 1975 *Waves in the Atmosphere*. Elsevier.

Kirby, J. T. & Chen, T.-M. 1989 Surface waves on vertically sheared flows: approximate dispersion relations. *J. Geophys. Res.* **94**, 1013–1027.

Lighthill, M. J. 1953 On the critical Froude number for turbulent flow over a smooth bottom. *Proc. Camb. Phil. Soc.* **49**, 704–706.

Lin, C. C. 1955 *The Theory of Hydrodynamic Stability*. Cambridge University Press.

Longuet-Higgins, M. S. 1998 Instabilities of a horizontal shear flow with a free surface. *J. Fluid Mech.* **364**, 147–162.

Miles, J. W. 1957 On the generation of surface waves by shear flows. *J. Fluid Mech.* **3**, 185–204.

Miles, J. W. 2001 A note on surface waves generated by shear-flow instability. *J. Fluid Mech.* **447**, 173–177.

Morland, L. C., Saffman, P. G. & Yuen, H. 1991 Waves generated by shear layer instabilities. *Proc. R. Soc. Lond.* A **413**, 441–450.

Pedlosky, J. 1982 *Geophysical Fluid Dynamics*. Springer.

Peregrine, D. H. 1976 Interaction of water waves and currents. *Adv. Appl. Mech.* **16**, 9–117.

Pullin, D. I. 1991 Contour dynamics method. *Annu. Rev. Fluid Mech.* **24**, 84–115.

Shrira, V. I. 1993 Surface waves on shear currents: solution of the boundary-value problem. *J. Fluid Mech.* **252**, 565–587.

Shrira, V. I. & Sazonov, I. A. 2001 Quasi-modes in boundary-layer-type flows. Part 1. Inviscid two-dimensional spatially harmonic perturbations. *J. Fluid Mech.* **446**, 133–171.

Skop, R. A. 1987 An approximate dispersion relation for wave-current interactions. *J. Waterway Port Coastal Ocean Engng*, **113**, 187–195.

Stern, M. E. & Adam, Y. A. 1973 Capillary waves generated by a shear current in water. *Mém. Soc. R. Sci. Liége*, **6e**, 6 série, 179–185.

Stewart, R. H. & Joy, J. W. 1974 HF radio measurements of surface currents. *Deep-Sea Res.* **21**, 1039–1049.

Terray, E. A., Donelan, M. A., Agrawal, Y. C., Drennan, W. M., Kahma, K. K., Kitaigorodskii, S. A., Hwang, P. A., & A. J. Williams, 3rd 1996 Estimates of kinetic energy dissipation under breaking waves. *J. Phys. Oceangr.* **26**, 792–807.

Thompson, P. D. 1949 The propagation of small surface disturbances through rotational flow. *Ann. NY Acad. Sci.* **51**, 463–474.

Triantyfallou, G. S. & Dimas, A. A. 1989 Interaction of two-dimensional separated flows with a free surface at low Froude numbers. *Phys. Fluids* A **1**, 1813–1821.

Wu, J. 1975 Wind-induced drift currents. *J. Fluid Mech.* **68**, 49–70.

Yih, C. S. 1972 Surface waves in flowing water. *J. Fluid Mech.* **51**, 209–220.